

# Highly efficient microwave memory using a superconducting artificial chiral atom

Kai-I Chu,<sup>1,\*</sup> Yung-Fu Chen,<sup>1,2</sup> and Wen-Te Liao<sup>1,2,3,†</sup>

<sup>1</sup>*Department of Physics, National Central University, Taoyuan City 32001, Taiwan*

<sup>2</sup>*Quantum Technology Center, National Central University, Taoyuan City 32001, Taiwan*

<sup>3</sup>*Physics Division, National Center for Theoretical Sciences, Taipei 10617, Taiwan*

(Dated: March 26, 2025)

A microwave memory using a superconducting artificial chiral atom embedded in a one-dimensional open transmission line is theoretically investigated. By applying a coupling field to a single artificial atom, we modify its dispersion, resulting in a slow probe pulse similar to electromagnetically induced transparency. The single atom's intrinsic chirality, along with optimal control of the coupling field, enables a storage efficiency exceeding 99% and near-unity fidelity across a broad range of pulse durations. Our scheme provides a feasible pathway toward highly efficient quantum information processing in superconducting circuits.

The superconducting circuit platform is a leading approach for realizing noisy intermediate-scale quantum processors [1–4]. To achieve fault-tolerant and scalable quantum computation, it is crucial to develop a quantum network [5–7] that interconnects multiple moderate-scale quantum processors through quantum communication and entanglement, enhancing computational capabilities and improving hardware efficiency. Within such a superconducting circuit-based network [8], microwave quantum memory - capable of storing and retrieving propagating quantum information - will be a key building block [9–11]. It enables synchronization and buffering of quantum information for parallel processing, improves computational efficiency, and facilitates quantum state transfer over intermediate distances in distributed superconducting quantum systems [12]. Additionally, it can support long-distance quantum teleportation [13] when required for large-scale quantum networks.

Recent approaches to microwave memory based on superconducting circuits coupling to high-coherence resonators can be categorized into three main schemes. The first approach invokes the atomic frequency comb, where an array of resonators absorbs the probe pulse [14–16]. Storage is achieved by either turning off the coupling between the information channel and the resonators [16] or by aligning the resonator frequencies [14]. The stored pulse is retrieved through an echo rephasing process. However, even if the resonators exhibit high coherence, the storage efficiency and fidelity are limited by deviations in the coupling strengths between the resonators and the information channel, variations in resonator frequencies and intrinsic losses, and impedance-matching conditions. Another challenge is that these memory devices typically require an additional circulator to transfer the stored information to another channel, which causes additional losses and further degrades the stored information [17]. The second approach employs directional absorption in a superconducting artificial molecule [18]. While this design enables directional control of the stored pulse, it requires complex control protocols and limits the spectral bandwidth of the stored pulse due to the excited-

state decay rate.

The third approach relies on electromagnetically induced transparency (EIT) using a three-level  $\Lambda$ -type superconducting-qubit-resonator system [19]. EIT mechanism slows down a probe pulse and renders the system transparent under the influence of the coupling light, due to quantum interference [20–22]. The probe pulse is stored in and retrieved from the high-coherence resonator by adiabatically switching the coupling light off and on. However, the storage efficiency is fundamentally limited by the small effective optical depth. A highly efficient EIT quantum memory requires a large optical depth, e.g., the world-record EIT quantum memory in cold-atom systems has an optical depth of approximately 550 [23]. A single superconducting atom has an effective optical depth of 2 only, and its theoretical maximum storage efficiency is 50% [24]. Moreover, in an open transmission line, the retrieved microwave propagates in both directions, further reducing the maximum storage efficiency to 25% [25].

In this letter, we address the above challenges and propose an EIT-like microwave memory using a superconducting artificial chiral atom embedded in a one-dimensional open transmission line. Here, chirality refers to the fact that the atomic scattering of the probe light depends on its propagation direction [26, 27]. Note that the transparency is essentially induced by the atomic chirality rather than the coupling field in the conventional EIT system. However, the coupling field still enables the slow probe light, and its dynamical control also leads to the memory effect [20–22]. Remarkably, our system exhibits an effective optical depth of only 4 and achieves high storage efficiency  $> 99\%$  and near-unity fidelity across a broad range of pulse durations. Moreover, our scheme does not need any circulator since the atom is embedded in an open transmission line. The propagating direction of the retrieved pulse can be controlled by adjusting the phase of the coupling light, which offers the versatility of our scheme for quantum information processing.

Our scheme is illustrated in Fig. 1(a). A pair of reso-

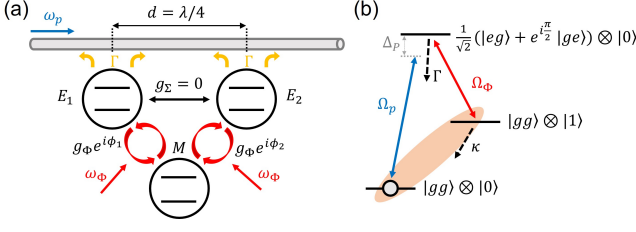


FIG. 1. (a) Schematic diagram of an artificial chiral atom embedded in a one-dimensional transmission line. The artificial atom consists of a pair of resonant emitter qubits  $E_1$  and  $E_2$  and a detuned memory qubit  $M$ .  $E_1$  and  $E_2$  are separated by  $\lambda/4$  with zero interaction ( $g_\Sigma = 0$ ), and they couple to  $M$  with controllable effective coupling strength  $g_\Phi e^{i\phi_{1(2)}}$  through the parametric modulations. (b) Energy-level diagram of the lowest three states of the chiral atom, forming an effective  $\Lambda$ -type system. The ground, excited, and metastable states are denoted as  $|gg\rangle \otimes |0\rangle$ ,  $(|eg\rangle + e^{i\pi/2} |ge\rangle)/\sqrt{2} \otimes |0\rangle$ , and  $|gg\rangle \otimes |1\rangle$ , respectively. A probe light is injected into the transmission line and couples to both emitters with Rabi frequency  $\Omega_p$  and detuning  $\Delta_p$ . The parametric modulations result in an effective coupling Rabi frequency  $\Omega_\Phi$ , which enables the transition between the excited and metastable states.

nant emitter qubits,  $E_1$  and  $E_2$ , with transition frequency  $\omega_e/2\pi = 5$  GHz couples to an open transmission line with a separation distance  $d = \lambda/4$ , where the wavelength  $\lambda = 2\pi c/\omega_e$ . This quarter-wavelength spacing prevents cooperative effects while maximizing the exchange coupling to  $J = \Gamma/2$  [28], where  $\Gamma/2\pi = 10$  MHz is the emitter relaxation rate. We assume that this exchange coupling  $J$  can be fully canceled by introducing a tunable coupler [29, 30], leading to a total coupling of  $g_\Sigma = 0$ . The absence of coupling results in fully directional emission and absorption of the emitter pair [18, 31]. In the weak probe regime, the excited state forms an entangled state,  $(|eg\rangle + e^{i\pi/2} |ge\rangle)/\sqrt{2}$ , due to time-reversal symmetry [18]. The phase sign is determined by the propagation direction of the probe light. Here, the probe is incident from the left. Additionally, each emitter is coupled to the same detuned high-coherence memory qubit or resonator,  $M$ , with transition frequency  $\omega_m/2\pi = 4$  GHz, positioned far from the transmission line. The coupling strength between the emitters and the memory qubit is smaller than their frequency difference, minimizing energy transfer from the memory qubit through the emitters to the transmission line. We treat these three quantum objects as a single chiral atom. The lowest three energy levels of the atom, depicted in Fig. 1(b), form an effective  $\Lambda$ -type structure with states  $|gg\rangle \otimes |0\rangle$ ,  $(|eg\rangle + e^{i\pi/2} |ge\rangle)/\sqrt{2} \otimes |0\rangle$ , and  $|gg\rangle \otimes |1\rangle$ , where  $|0\rangle$  and  $|1\rangle$  denote the ground and excited states of the memory qubit, respectively. The state  $|gg\rangle \otimes |1\rangle$  serves as the metastable state of the atom, which is used for microwave storage.

To map the weak resonant probe light with frequency  $\omega_p = \omega_e$  and Rabi frequency  $\Omega_p$  onto the coherence of

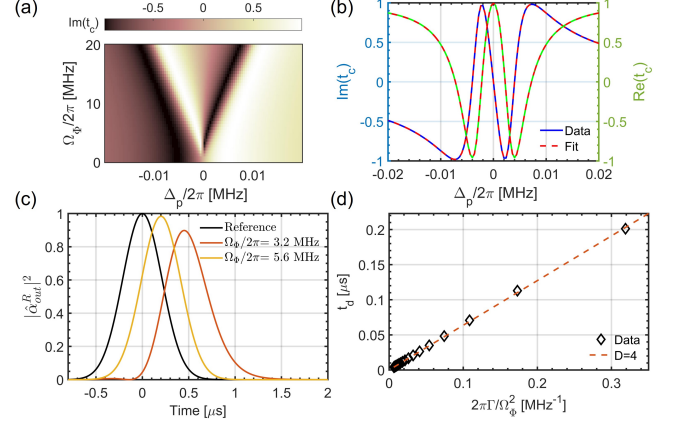


FIG. 2. (a) The imaginary part of the probe transmission coefficient  $\text{Im}(t_c)$  as a function of  $\Delta_p$  and  $\Omega_\Phi$ .  $\gamma_\phi/2\pi = 0.1$  MHz and  $\Gamma_m/2\pi = 4$  kHz are considered. (b) Blue-solid (Green-solid) line depicts  $\Delta_p$ -dependent imaginary (real) part of  $t_c$  for  $\Omega_\Phi/2\pi = 8$  MHz. Dashed lines represent the theoretical curve. (c) Slow probe light signal  $|a_{out}^R|^2$  for  $\Omega_\Phi/2\pi = 3.2$  MHz (yellow-solid line) and 5.6 MHz (red-solid line). The black-solid line is the input probe pulse. (d) Group delay time  $t_d$  as a function of  $\Omega_\Phi$ . The black open diamonds represent data extracted from (c), and the red dashed line illustrates the EIT delay-time formula  $4\Gamma/\Omega_\Phi^2$ .

the metastable state, the otherwise forbidden transition between the emitters and the memory qubit must be activated [32]. This is achieved using a parametric modulation technique [33–35], which modulates the emitters' transition frequency at  $\omega_\Phi = \omega_e - \omega_m$ . The modulation induces an effective coupling strength  $g_\Phi e^{i\phi_{1(2)}}$  between the emitters and the memory qubit, where  $\phi_{1(2)}$  represents the modulation phase for emitter 1(2) and the memory qubit. Furthermore, the phase difference must be set to  $\phi \equiv \phi_1 - \phi_2 = -\pi/2$ , ensuring a non-reciprocal effect [36] for the two-photon resonant probe incident from the left. This can be understood as the memory qubit, under parametric modulations, forming a path-entangled state with a specific phase  $\phi$ , where the excitation is transferred to one of the emitters while remaining indistinguishable between them. The emission from the emitters occurs only to the right due to the interference effect governed by  $\phi$  and the propagation phase accumulation over  $d = \lambda/4$ . As a result, these two modulations collectively act as a resonant coupling light, resulting in an effective Rabi frequency  $\Omega_\Phi$ , which facilitates the transition from the excited state to the metastable state of the chiral atom, as we will see later.

We first characterize the optical response of the weak probe light with  $\Omega_p = 0.01\Gamma$ . The Hamiltonian describing the interaction between the probe light and the chiral atom under the coupling light, within the rotating frame

approximation [31, 37], is given by

$$H = \sum_{i=1,2} (\omega_e - \omega_p) \sigma_i^\dagger \sigma_i + (\omega_m - \omega_p + \omega_\Phi) \sigma_m^\dagger \sigma_m + g_\Phi (e^{i\phi} \sigma_1^\dagger \sigma_m + \sigma_2^\dagger \sigma_m) + \frac{\Omega_p}{2} (\sigma_1^\dagger + e^{ikd} \sigma_2^\dagger) + \text{H.c.}, \quad (1)$$

where  $\sigma_{1(2)}$  denotes the lowering operator for the emitter 1(2),  $\sigma_m$  is the lowering operator for the memory qubit, and  $k$  is the wavevector of the probe light. The time evolution of the system is governed by the Lindblad master equation,

$$\dot{\rho} = -i[H, \rho] + \sum_{i=1,2} \frac{\Gamma}{2} \mathcal{D}[\sigma_i] \rho + \gamma_\phi \mathcal{D}[\sigma_i^\dagger \sigma_i] \rho + \frac{\Gamma_m}{2} \mathcal{D}[\sigma_m], \quad (2)$$

where  $\mathcal{D}[\mathcal{O}]\rho = 2\mathcal{O}\rho\mathcal{O}^\dagger - \rho\mathcal{O}^\dagger\mathcal{O} - \mathcal{O}^\dagger\mathcal{O}\rho$  is the dissipator, and  $\rho(t)$  is the system's density matrix. The dynamics of the density matrix is solved using QuTiP [38]. We also account for the emitters' pure dephasing rate  $\gamma_\phi$  and the memory qubit's loss rate  $\Gamma_m$ . To determine the output field propagating to the right, we use the input-output formalism, where the output coherent field is given by [18, 28, 31]

$$\hat{a}_{out}^R = \hat{a}_{in}^R + \sqrt{\frac{\Gamma}{2}} (\sigma_1 + \sigma_2 e^{-i\frac{\pi}{2}}). \quad (3)$$

The steady-state transmission coefficient is defined as  $t_c = \hat{a}_{out}^R / \hat{a}_{in}^R$ , where the input coherent field is given by  $\hat{a}_{in}^R = \Omega_p / \sqrt{2\Gamma}$ . The real and imaginary parts of  $t_c$  are plotted as a function of the probe detuning  $\Delta_p = \omega_e - \omega_p$  with resonant coupling light in Fig. 2(b). The data can be well described by the following analytical expression for the transmission coefficient [39]:

$$t_c^a = 1 + 2i \frac{\frac{\Gamma}{2} (\Delta_p - i\frac{\Gamma_m}{2})}{(\Delta_p - i\frac{\Gamma_m}{2})(\Delta_p - i\gamma) - (\frac{\Omega_\Phi^2}{4})}, \quad (4)$$

where  $\gamma = \gamma_\phi + \Gamma/2$  is the total decoherence rate of the emitters. By fitting the data in Fig. 2(a) and (b) to Eq. 4, we find that the condition  $\Omega_\Phi = 2\sqrt{2}g_\Phi$  holds, where Fig. 2(a) illustrates how  $\text{Im}(t_c)$  varies with  $\Delta_p$  and  $\Omega_\Phi$ . This tunable dispersion indicates that the group delay time  $t_d$  of the probe can be controlled by adjusting  $\Omega_\Phi$ . The slow-light effect is measured by sending a Gaussian probe pulse,  $\Omega_p(t) = \Omega_p \exp(-t^2/2\tau_s^2)$ , with a duration of  $\tau_s = 300$  ns into the atom under continuous coupling light. The result is shown in Fig. 2(c). As  $\Omega_\Phi$  decreases,  $t_d$  increases due to the steepening of the dispersion. To determine the effective optical depth  $D$  of the chiral atom, we analyze  $t_d$  as a function of  $\Omega_\Phi$  in Fig. 2(d) and compare it with the expression  $t_d = D\Gamma/\Omega_\Phi^2$ , commonly used in atomic systems. The result indicates that the optical depth has increased to  $D = 4$ , compared to previous work [19, 25].

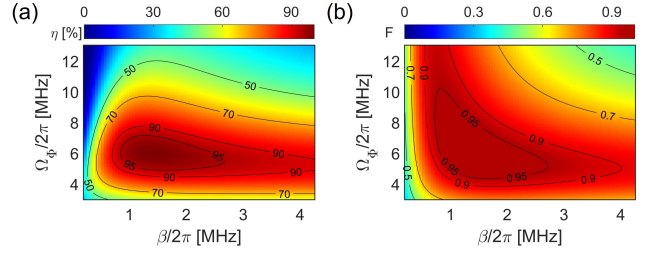


FIG. 3. (a) Storage efficiency  $\eta$  and (b) fidelity  $F$  as functions of  $\Omega_\Phi$  and switching slope  $\beta$ .

To study the light storage process, we adiabatically turn off and on the coupling light while the probe pulse is within the atomic medium. The dynamics of the coupling function is given by

$$\Omega_c(t) = \frac{\Omega_\Phi}{2} ([1 - \tanh \beta(t - t_{off})] + [1 + \tanh \beta(t - t_{on})]), \quad (5)$$

where  $\beta$ ,  $t_{off}$ , and  $t_{on}$  represent the slope, turn-off time, and turn-on time, respectively. Fig. 3(a) shows the storage efficiency  $\eta$  of a  $\tau_s = 100$  ns probe pulse with  $t_{off} = 80$  ns, defined as

$$\eta = \frac{\int_{t_{on}}^{\infty} |\hat{a}_{out}^R|^2 dt}{\int_{-\infty}^0 |\hat{a}_{in}^R|^2 dt}, \quad (6)$$

as a function of  $\Omega_\Phi$  and  $\beta$  under the ideal case where no dephasing or loss is considered. A near-100 % efficiency is observed, indicating that the probe pulse is fully compressed into the atom. Notably, the full compression of the pulse is not solely due to the interference effect via the coupling light, but also results from the chiral interference effect. Otherwise, if the medium had only an optical depth of  $D = 4$ , the maximum achievable efficiency would be limited to 75 % [24]. The classical fidelity  $F$ , defined as the similarity between the retrieved and input pulses, is given by [40]

$$F = \frac{|\int \hat{a}_{in}^{R*}(t) \hat{a}_{out}^R(t - t') dt|^2}{\int |\hat{a}_{in}^R|^2 dt \int |\hat{a}_{out}^R|^2 dt}, \quad (7)$$

where  $t'$  denotes the time of the maximum amplitude of the retrieved pulse. As shown in Fig. 3(b), the fidelity also approaches unity. The optimized values of  $\eta$  and  $F$  indicate how to fine-tune the control parameters of  $\Omega_c$ , to achieve optimal storage and retrieval performance.

To study the practical performance of light storage, we compute the optimized storage and retrieval dynamics while considering the effects of dephasing and loss.  $\gamma_\phi$  and  $\Gamma_m$  take the same values as those used in Fig. 2. We define the storage time as  $\tau_d = t_{on} - t_{off} - 5\beta^{-1}$ , ensuring that the probe pulse is fully inside the medium. Fig. 4(a) presents the time evolution of the probe pulse and the coherence of the metastable state for a storage time of  $\tau_d = 1 \mu\text{s}$ . As the coupling light is adiabatically turned off, the probe pulse is mapped onto

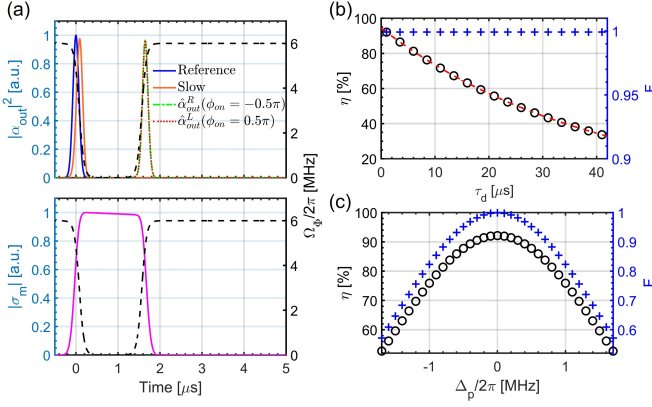


FIG. 4. (a) Optimized storage and retrieval sequence. The upper plot shows the output probe signal  $|\alpha_{\text{out}}|^2$ . The black-dashed line represents the control sequence of the coupling light. The orange line denotes the slow probe light under constant  $\Omega_{\Phi}/2\pi = 6$  MHz. The blue line is the input probe pulse. The green and red-dotted lines depict the retrieved pulses propagating in opposite directions, achieved by tuning the turned-on phase difference  $\phi_{\text{on}}$  of the two parametric modulations. The lower plot shows the transformation between the microwave coherence and the memory qubit coherence  $\sigma_m$ . (b)  $\eta$  (black-empty circles) and  $F$  (blue cross symbols) as functions of the storage time  $\tau_d$ . The red dashed line represents the exponential decay fitting. (c)  $\eta$  (black circle) and  $F$  (blue cross) as functions of  $\Delta_p$  for storage time of  $\tau_d = 1$   $\mu\text{s}$ .

the coherence of the metastable state, demonstrating the EIT storage mechanism. Moreover, the retrieved pulse's propagation direction can be controlled by adjusting the phase difference  $\phi_{\text{on}}$  of the turned-on parametric modulations. The left-propagating coherent field is calculated as  $\hat{a}_{\text{out}}^L = \sqrt{\Gamma/2}(\sigma_1 + \sigma_2 e^{+i\pi/2})$ . The results show that the controllable  $\phi_{\text{on}}$  induces an effect similar to the use of different propagation directions of coupling light in atomic systems for controlling the direction of the retrieved pulse [41].  $\eta$  and  $F$  are plotted as functions of  $\tau_d$  in Fig. 4(b). The decay of  $\eta$  is governed by the coherence time of the metastable state, with fitting results indicating a decay rate equal to  $\Gamma_m$ . However,  $F$  remains near unity even in the presence of decoherence, suggesting that the retrieved pulse retains high phase coherence despite energy loss.

Since the emitters should be fixed at a  $\lambda/4$  distance, the excited state of the atom lacks frequency tunability. Therefore, it is crucial to study the memory bandwidth, which determines how efficiently the system can store signals at different input detunings. Fig. 4(c) illustrates  $\eta$  and  $F$  as functions of  $\Delta_p$ , under the same control conditions as Fig. 4(a). Our results indicate that the storage bandwidth is approximately 3.4 MHz, defined as the detuning range over which  $\eta$  remains above 50%. Within this range, the retrieved pulse fidelity can still remain above 0.5.

Finally, we study how the optimized  $\eta$  and  $F$  vary with  $\tau_s$ , as shown in Fig. 5, while keeping  $t_{\text{off}} = 0$  fixed

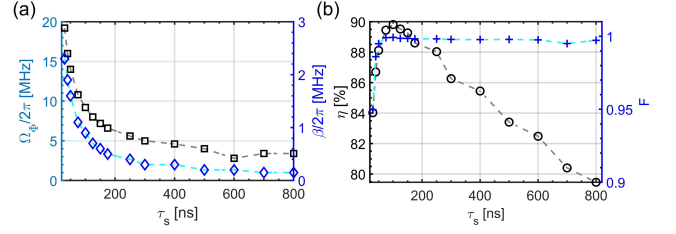


FIG. 5. (a) Optimized coupling-field  $\Omega_{\Phi}$  (black empty squares) and  $\beta$  (blue empty diamonds) by maximizing  $\eta$  for different input probe pulse duration  $\tau_s$ . (b) Optimal  $\eta$  (black empty circles) and  $F$  (blue cross symbols) as functions of  $\tau_s$ .

throughout the examination. We find that for longer pulses, both  $\Omega_{\Phi}$  and  $\beta$  need to be smaller to ensure the entire pulse is fully compressed within the medium. In Fig. 5(b), we observe that  $F$  remains near unity as  $\tau_s$  increases, while  $\eta$  decreases due to the finite coherence time of the memory qubit. However, for shorter pulses (around 50 ns), both of them drop significantly. This occurs because the pulse spectral bandwidth overlaps with the dressed-state absorption peaks, leading to a quantum-beating effect. In the short-pulse regime, an Autler-Townes splitting-based quantum memory approach could help mitigate this issue and may also be applicable to our chiral atom system [42, 43].

In conclusion, we propose a highly efficient EIT-like microwave memory based on a superconducting artificial chiral atom embedded in an open transmission line. The scheme achieves a storage efficiency of up to 99% and near-unity fidelity, enabled by the atom's chirality and quantum interference. The propagation direction of the retrieved pulse can also be precisely controlled. Relying on interference effects, the memory operates with a simple adiabatic control protocol and supports a wide range of pulse durations compared to Ref. [18]. Moreover, our method requires only a single memory qubit, avoiding the performance degradation associated with deviations in resonator array implementations [14–16]. The EIT-based protocol also enables the storage of arbitrary waveforms, provided their spectral bandwidth lies within the EIT window. By using only a single artificial atom, our scheme contrasts with conventional atomic systems that depend on large optical depths. These results demonstrate a promising approach for achieving highly efficient microwave memory in superconducting circuits.

The work was supported by the National Science and Technology Council in Taiwan through Grants No. NSTC 113-2112-M-008-006, NSTC-110-2112-M-008-027-MY3, NSTC-111-2923-M-008-004-MY3 and NSTC-111-2639-M-007-001-ASP.

- \* Correspondence to: kaiichu0903@gmail.com  
 † Correspondence to: wente.liao@g.ncu.edu.tw
- [1] M. H. Devoret and R. J. Schoelkopf, Superconducting circuits for quantum information: an outlook, *Science* **339**, 1169 (2013).
  - [2] F. Arute, K. Arya, R. Babbush, D. Bacon, J. C. Bardin, R. Barends, R. Biswas, S. Boixo, F. G. Brandao, D. A. Buell, *et al.*, Quantum supremacy using a programmable superconducting processor, *Nature* **574**, 505 (2019).
  - [3] M. Kjaergaard, M. E. Schwartz, J. Braumüller, P. Krantz, J. I.-J. Wang, S. Gustavsson, and W. D. Oliver, Superconducting qubits: Current state of play, *Annual Review of Condensed Matter Physics* **11**, 369 (2020).
  - [4] D. Gao, D. Fan, C. Zha, J. Bei, G. Cai, J. Cai, S. Cao, F. Chen, J. Chen, K. Chen, *et al.*, Establishing a new benchmark in quantum computational advantage with 105-qubit zuchongzhi 3.0 processor, *Physical Review Letters* **134**, 090601 (2025).
  - [5] H. J. Kimble, The quantum internet, *Nature* **453**, 1023 (2008).
  - [6] S. Wehner, D. Elkouss, and R. Hanson, Quantum internet: A vision for the road ahead, *Science* **362**, eaam9288 (2018).
  - [7] S.-H. Wei, B. Jing, X.-Y. Zhang, J.-Y. Liao, C.-Z. Yuan, B.-Y. Fan, C. Lyu, D.-L. Zhou, Y. Wang, G.-W. Deng, *et al.*, Towards real-world quantum networks: a review, *Laser & Photonics Reviews* **16**, 2100219 (2022).
  - [8] P. Magnard, S. Storz, P. Kurpiers, J. Schär, F. Marxer, J. Lütolf, T. Walter, J.-C. Besse, M. Gabureac, K. Reuer, *et al.*, Microwave quantum link between superconducting circuits housed in spatially separated cryogenic systems, *Physical review letters* **125**, 260502 (2020).
  - [9] A. I. Lvovsky, B. C. Sanders, and W. Tittel, Optical quantum memory, *Nature photonics* **3**, 706 (2009).
  - [10] K. Heshami, D. G. England, P. C. Humphreys, P. J. Bustard, V. M. Acosta, J. Nunn, and B. J. Sussman, Quantum memories: emerging applications and recent advances, *Journal of modern optics* **63**, 2005 (2016).
  - [11] C. Liu, M. Wang, S. A. Stein, Y. Ding, and A. Li, Quantum memory: A missing piece in quantum computing units, *arXiv preprint arXiv:2309.14432* (2023).
  - [12] M. Caleffi, M. Amoretti, D. Ferrari, J. Illiano, A. Manzalini, and A. S. Cacciapuoti, Distributed quantum computing: a survey, *Computer Networks* **254**, 110672 (2024).
  - [13] L.-M. Duan, M. D. Lukin, J. I. Cirac, and P. Zoller, Long-distance quantum communication with atomic ensembles and linear optics, *Nature* **414**, 413 (2001).
  - [14] Z. Bao, Z. Wang, Y. Wu, Y. Li, C. Ma, Y. Song, H. Zhang, and L. Duan, On-demand storage and retrieval of microwave photons using a superconducting multi-resonator quantum memory, *Physical Review Letters* **127**, 010503 (2021).
  - [15] A. R. Matanin, K. I. Gerasimov, E. S. Moiseev, N. S. Smirnov, A. I. Ivanov, E. I. Malevannaya, V. I. Polozov, E. V. Zikiy, A. A. Samoilov, I. A. Rodionov, *et al.*, Toward highly efficient multimode superconducting quantum memory, *Physical Review Applied* **19**, 034011 (2023).
  - [16] T. Makihara, N. Lee, Y. Guo, W. Guan, and A. Safavi-Naeini, A parametrically programmable delay line for microwave photons, *Nature Communications* **15**, 4640 (2024).
  - [17] S. Moiseev, K. Gerasimov, R. Latypov, N. Perminov, K. Petrovnin, and O. Sherstyukov, Broadband multi-resonator quantum memory-interface, *Scientific reports* **8**, 3982 (2018).
  - [18] N. Gheeraert, S. Kono, and Y. Nakamura, Programmable directional emitter and receiver of itinerant microwave photons in a waveguide, *Physical Review A* **102**, 053720 (2020).
  - [19] K.-I. Chu, X.-C. Lu, K.-H. Chiang, Y.-H. Lin, C.-D. Chen, I. A. Yu, W.-T. Liao, and Y.-F. Chen, Slow and stored light via electromagnetically induced transparency using a  $\lambda$ -type superconducting artificial atom, *Physical Review Research* **7**, L012015 (2025).
  - [20] M. Fleischhauer and M. D. Lukin, Dark-state polaritons in electromagnetically induced transparency, *Physical review letters* **84**, 5094 (2000).
  - [21] D. F. Phillips, A. Fleischhauer, A. Mair, R. L. Walsworth, and M. D. Lukin, Storage of light in atomic vapor, *Physical review letters* **86**, 783 (2001).
  - [22] M. Fleischhauer, A. Imamoglu, and J. P. Marangos, Electromagnetically induced transparency: Optics in coherent media, *Reviews of modern physics* **77**, 633 (2005).
  - [23] Y.-F. Hsiao, P.-J. Tsai, H.-S. Chen, S.-X. Lin, C.-C. Hung, C.-H. Lee, Y.-H. Chen, Y.-F. Chen, I. A. Yu, and Y.-C. Chen, Highly efficient coherent optical memory based on electromagnetically induced transparency, *Physical review letters* **120**, 183602 (2018).
  - [24] A. V. Gorshkov, A. André, M. D. Lukin, and A. S. Sørensen, Photon storage in  $\lambda$ -type optically dense atomic media. ii. free-space model, *Physical Review A* **76**, 033805 (2007).
  - [25] K.-I. Chu, W.-T. Liao, and Y.-F. Chen, Three-level  $\lambda$ -type microwave memory via parametric-modulation-induced transparency in a superconducting quantum circuit, *Physical Review Research* **5**, 033192 (2023).
  - [26] P. Lodahl, S. Mahmoodian, S. Stobbe, A. Rauschenbeutel, P. Schneeweiss, J. Volz, H. Pichler, and P. Zoller, Chiral quantum optics, *Nature* **541**, 473 (2017).
  - [27] C. Joshi, F. Yang, and M. Mirhosseini, Resonance fluorescence of a chiral artificial atom, *Physical Review X* **13**, 021039 (2023).
  - [28] K. Lalumiere, B. C. Sanders, A. F. van Loo, A. Fedorov, A. Wallraff, and A. Blais, Input-output theory for waveguide qed with an ensemble of inhomogeneous atoms, *Physical Review A* **88**, 043806 (2013).
  - [29] F. Yan, P. Krantz, Y. Sung, M. Kjaergaard, D. L. Campbell, T. P. Orlando, S. Gustavsson, and W. D. Oliver, Tunable coupling scheme for implementing high-fidelity two-qubit gates, *Physical Review Applied* **10**, 054062 (2018).
  - [30] X. Li, T. Cai, H. Yan, Z. Wang, X. Pan, Y. Ma, W. Cai, J. Han, Z. Hua, X. Han, *et al.*, Tunable coupler for realizing a controlled-phase gate with dynamically decoupled regime in a superconducting circuit, *Physical Review Applied* **14**, 024070 (2020).
  - [31] B. Kannan, A. Almanakly, Y. Sung, A. Di Paolo, D. A. Rower, J. Braumüller, A. Melville, B. M. Niedzielski, A. Karamlou, K. Serniak, *et al.*, On-demand directional microwave photon emission using waveguide quantum electrodynamics, *Nature Physics* **19**, 394 (2023).
  - [32] A. Blais, J. Gambetta, A. Wallraff, D. I. Schuster, S. M.

- Girvin, M. H. Devoret, and R. J. Schoelkopf, Quantum-information processing with circuit quantum electrodynamics, *Physical Review A* **75**, 032329 (2007).
- [33] J. Strand, M. Ware, F. Beaudoin, T. Ohki, B. Johnson, A. Blais, and B. Plourde, First-order sideband transitions with flux-driven asymmetric transmon qubits, *Physical Review B—Condensed Matter and Materials Physics* **87**, 220505 (2013).
- [34] D. C. McKay, S. Filipp, A. Mezzacapo, E. Magesan, J. M. Chow, and J. M. Gambetta, Universal gate for fixed-frequency qubits via a tunable bus, *Physical Review Applied* **6**, 064007 (2016).
- [35] S. Caldwell, N. Didier, C. Ryan, E. Sete, A. Hudson, P. Karalekas, R. Manenti, M. da Silva, R. Sinclair, E. Acala, *et al.*, Parametrically activated entangling gates using transmon qubits, *Physical Review Applied* **10**, 034050 (2018).
- [36] X. Cao, A. Irfan, M. Mollenhauer, K. Singirikonda, and W. Pfaff, Parametrically controlled chiral interface for superconducting quantum devices, *Physical Review Applied* **22**, 064023 (2024).
- [37] M. Kervinen, J. E. Ramírez-Muñoz, A. Välimaa, and M. A. Sillanpää, Landau-zener-stückelberg interference in a multimode electromechanical system in the quantum regime, *Physical review letters* **123**, 240401 (2019).
- [38] J. R. Johansson, P. D. Nation, and F. Nori, Qutip: An open-source python framework for the dynamics of open quantum systems, *Computer physics communications* **183**, 1760 (2012).
- [39] X. Gu, A. F. Kockum, A. Miranowicz, Y.-x. Liu, and F. Nori, Microwave photonics with superconducting quantum circuits, *Physics Reports* **718**, 1 (2017).
- [40] Y.-H. Chen, M.-J. Lee, I.-C. Wang, S. Du, Y.-F. Chen, Y.-C. Chen, and I. A. Yu, Coherent optical memory with high storage efficiency and large fractional delay, *Physical review letters* **110**, 083601 (2013).
- [41] Y.-W. Lin, W.-T. Liao, T. Peters, H.-C. Chou, J.-S. Wang, H.-W. Cho, P.-C. Kuan, and I. A. Yu, Stationary light pulses in cold atomic media and without bragg gratings, *Physical review letters* **102**, 213601 (2009).
- [42] W.-T. Liao, C. H. Keitel, and A. Pálffy, All-electromagnetic control of broadband quantum excitations using gradient photon echoes, *Physical review letters* **113**, 123602 (2014).
- [43] E. Saglamyurek, T. Hrushevskiy, A. Rastogi, K. Heshami, and L. J. LeBlanc, Coherent storage and manipulation of broadband photons via dynamically controlled autler–townes splitting, *Nature Photonics* **12**, 774 (2018).